Analysis of oil film interferometry implementation in non-ideal conditions

Kevin Chen

January 7, 2010

Abstract

An analytical study is done to explain the effects of certain imperfect conditions on the implementation of oil film interferometry. After a review of classical thin film theory as it pertains to oil film interferometry, an analysis is given for a flat 1-D wall surface roughness, hysteresis when the applied wind shear changes, and the linear error propagation from temperature. It is found that the experimental technique is robust to 1-D surface roughness, because the oil film thickness obeys the same underlying equations as the classical theory. Two examples are given. Furthermore, a scaling argument shows that an instantaneous change in applied shear stress would create a new steady state in the oil film within a mere fraction of a second; therefore hysteresis is negligible. Finally, error analysis shows that for typical silicone oils, every degree Celsius of temperature error creates a -2.2% error in the calculated shear stress. Therefore, accurate temperature sensing is an absolute requirement for this technique.

1 Introduction

Oil film interferometry is a wind tunnel technique used to measure shear stress at a wall. It is commonly employed in boundary layer studies because it is easy to employ and does not require calibration [1]. Furthermore, the method is fairly unintrusive [2], which makes it an attractive option for wall shear stress measurement.

In this method, an silicone oil drop is placed on a reflective surface where the shear stress is to be measured. As the wind tunnel operates, the drop blows downstream, leaving behind a thin film. The shear stress determines the geometry of the film through a relation derived from the thin film equation, using the shear stress as an upper boundary condition on the film. When a monochromatic light source such as a sodium lamp or a laser illuminates the oil film from above,

some of the light will reflect off the oil surface; the other part will transmit through the oil, reflect off the wall, and transmit back to the air. This creates a constructive and destructive interference fringe pattern on the film. Since the fringes are level sets of the film thickness (based on the light source's optical wavelength in the oil), the shear stress can be extrapolated from image data. An example of this is shown in Figure 1, taken from an experiment in the Lucas Wind Tunnel at the California Institute of Technology [3].

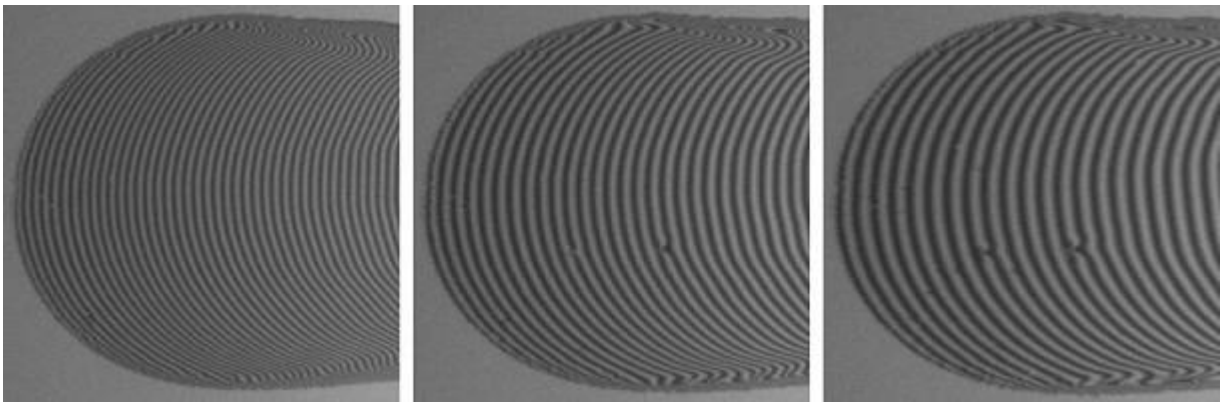

Figure 1: An example of an application of oil film interferometry, used here to measure the shear stress in a boundary layer downstream of a turbulence grid [3]. Wind blows from left to right and shears the oil film. The shear stress can be calculated from oil specifications and from the rate of change of fringe spacing on the oil.

The physics behind the technique were laid out by Squire in 1961 [2]. Tanner and Blows' seminal 1976 article [4] was the first to describe the practical implementation, and it provided an analysis and discussion of experimental considerations. In the most general case, when an oil film spreads on a flat surface with a steady, zero pressure gradient flow parallel to the surface, the shear stress is given by

$$\tau = \frac{2n\mu}{\lambda}\frac{ds}{dt}, \tag{1}$$

where n is the silicone oil's index of refraction, μ is the oil viscosity, λ is the wavelength of the monochromatic light source in a vacuum, and $\frac{ds}{dt}$ is the rate of change of fringe spacing on the film [5].

It is important to note, however, that equation (1) is built on several assumptions, which are described in Section 2.2. The oil film is assumed to be nominally one-dimensional; that is, two-dimensional effects are not considered. Gravitational, surface tension, and inertial effects are

neglected, and the lubrication approximation must be made. The shear stress is assumed to be constant in space and time, and pressure gradients in the airflow are taken to be zero.

To some degree, the model remains robust despite the assumptions. For instance, Naughton [6] explained that neglecting inertial, capillary, and pressure gradient effects is usually a reasonable assumption. Tanner [4] demonstrated that forces unaccounted for in the basic oil film theory (e.g., capillary forces) may produce perturbations, but these perturbations decay with time. Janke [7] and Fernholz [1] considered shear stresses that may fluctuate in time and space (i.e., $\tau(x,t) = \bar{\tau}(x) + \Delta\tau(x,t)$, with $\bar{\tau}$ the time average), and the former showed that the film geometry is generally unaffected by the temporal fluctuation $\Delta\tau$.

Nevertheless, it is necessary to analyze how certain experimental conditions may require a correction on equation (1). Squire [2] analytically showed that oil film interferometry would predict the point of separation too far upstream. Tanner [4] experimentally tested the use of oil film interferometry in a separating boundary layer, and he determined adjustments that are required near the separation point. In addition, Tanner characterized the effect of a pressure gradient $\frac{dp}{dx}$ if the gradient is small, or alternatively if $\tau = 0$; he also considered alternate wall geometries, such as sloped or curved surfaces.

In this study, we consider additional deviations from the aforementioned assumptions, and we analyze the impact on the application of the experimental technique. After reviewing the derivation of the oil film interferometry equation, we consider the effect on the oil film and on the experimental technique when a 1-D surface roughness is present. This is motivated in part by the implantation of airborne debris in the oil film, which is a common problem in the implementation

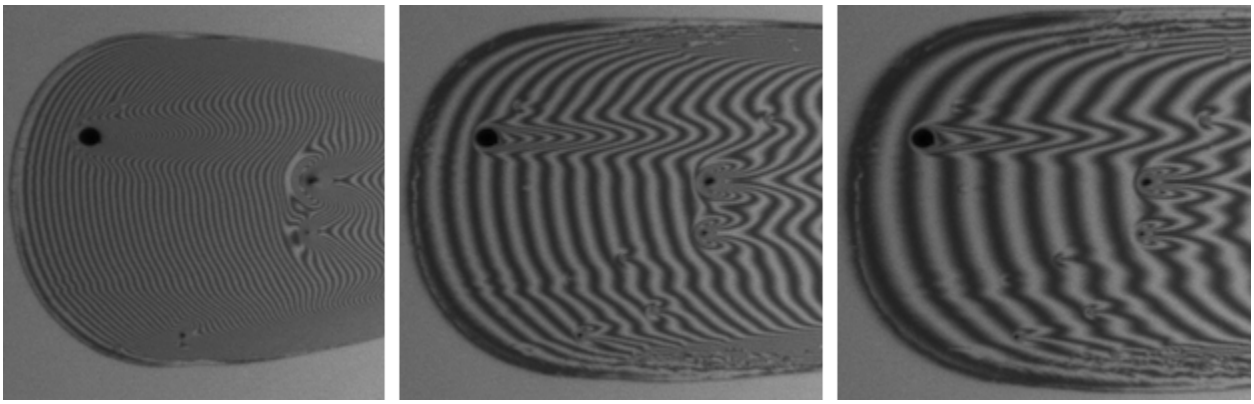

Figure 2: Oil film contaminated with previously airborne debris [3]. Compare with Figure 1.

of this technique (see Figure 2). The study of airborne debris effects likely requires a fully 3-D numerical simulation, so we turn instead to the simpler problem of a 1-D surface roughness whose height scale is small compared to the thickness of the film. In addition, we discuss two minor topics—whether hysteresis is significant when the applied shear stress changes, and the degree to which temperature measurement error propagates into the calculated shear stress. These are both relevant and practical topics in the application of oil film interferometry.

2 Theory

2.1 Nondimensionalization

The full solution for the 1-D oil film height can be expressed as $h = h\left(x, t; \tau, \mu, \rho g, \gamma\right)$. In Section 2.2, we find that the ρg and γ terms alter the dynamics in a negligible way. We can only apply this *a priori* if we have the foresight to know that the film will in general be very flat and very thin. Thus, the dependence reduces to $h = h\left(x, t; \tau, \mu\right)$. Observing this, we note immediately that this problem contains no natural length scale. Thus, we can reason that h is proportional to x; specifically, $h = x\, f\left(\frac{\tau t}{\mu}\right)$, which is confirmed in Section 2.2.

Nevertheless, for the purpose of generalizing the derivation procedure to cases where there may exist other length scales (e.g., a 1-D surface roughness), we assign an arbitrary constant inverse length k for the purpose of nondimensionalizing lengths. The reason for this choice will become clear in the examples in Sections 3.2 and 3.3. Using this length scale, we can define

$$\hat{h} \equiv kh \qquad \hat{x} \equiv kx \qquad \hat{y} \equiv ky \qquad \hat{t} \equiv \frac{\tau t}{\mu} \qquad \hat{u} \equiv \frac{k\mu u}{\tau} \qquad \hat{g} \equiv \frac{\rho g}{k\tau} \qquad \hat{\gamma} \equiv \frac{k\gamma}{\tau} \qquad \hat{p} \equiv \frac{p}{\tau} \tag{2}$$

so that $\hat{h} = \hat{h}\left(\hat{x}, \hat{t}\right)$ in the reduced problem, and $\hat{h} = \hat{h}\left(\hat{x}, \hat{t}; \hat{g}, \hat{\gamma}\right)$ in the full problem. Nevertheless, caution must be exercised when using this nondimensional scheme; this method may only be practical when the wind-imposed shear τ is assumed to be a constant.

2.2 Derivation

The oil film interferometry equation (1) is derived in a similar manner to the standard 1-D thin film equation, but the free surface boundary condition must be changed to account for the wind

shear, and gravitational and surface tension effects must be neglected. In practice, inertial terms can be neglected when analyzing the motion of an oil drop in a wind shear. Even in high wind tunnel speeds, the speed and length scales associated with the oil drop are very small compared to the viscous diffusion scale of the oil. Furthermore, the lubrication approximation can be applied because of the typically micrometer-scale thickness of the oil film. This allows us to argue, for instance, that $\frac{\partial^2 u}{\partial y^2} \gg \frac{\partial^2 u}{\partial x^2}$ and thus $\frac{\partial^2 \hat{u}}{\partial \hat{y}^2} \gg \frac{\partial^2 \hat{u}}{\partial \hat{x}^2}$, and that $\hat{v} \approx 0$.

Given a film height $\hat{h}\left(\hat{x},\hat{t}\right)$ and oil $\hat{x}$-velocity $\hat{u}\left(\hat{x},\hat{y},\hat{t}\right)$, with $\hat{x}$ in the direction of the wind shear and $\hat{y}$ in the vertical direction, continuity and x- and y-momentum yield

$$0 = \frac{\partial \hat{h}}{\partial \hat{t}} + \frac{\partial}{\partial \hat{x}}\left(\hat{h}\langle\hat{u}\rangle\right) \tag{3}$$

$$0 = -\frac{\partial \hat{p}}{\partial \hat{x}} + \frac{\partial^2 \hat{u}}{\partial \hat{y}^2} \tag{4}$$

$$0 = -\frac{\partial \hat{p}}{\partial \hat{y}} - \hat{g} \tag{5}$$

where $\langle\hat{u}\rangle \equiv \hat{h}^{-1}\int_0^{\hat{h}} \hat{u}\, d\hat{y}$. This is subject to boundary conditions

$$0 = \hat{u}\left(\hat{x},0,\hat{t}\right) \qquad \text{(no-slip)} \tag{6}$$

$$1 = \frac{\partial \hat{u}}{\partial \hat{y}}\left(\hat{x},\hat{h}\left(\hat{x},\hat{t}\right),\hat{t}\right). \qquad \text{(wind-imposed shear)} \tag{7}$$

Equation (5) implies $\frac{\partial^2 \hat{p}}{\partial \hat{x}\partial \hat{y}} = 0$, and hence $\frac{\partial \hat{p}}{\partial \hat{x}}$ has no dependence on $\hat{y}$. Thus, integrating equation (4) twice in $\hat{y}$ and applying the two boundary conditions yields

$$\hat{u}\left(\hat{x},\hat{y},\hat{t}\right) = \frac{\hat{y}^2}{2}\frac{\partial \hat{p}}{\partial \hat{x}} + \hat{y}\left(1 - \frac{\partial \hat{p}}{\partial \hat{x}}\hat{h}\right); \tag{8}$$

from this, we find

$$\langle\hat{u}\rangle\left(\hat{x},\hat{t}\right) = -\frac{\hat{h}^2}{3}\frac{\partial \hat{p}}{\partial \hat{x}} + \frac{\hat{h}}{2}. \tag{9}$$

Substituting this in the continuity equation (3), we find

$$\frac{\partial \hat{h}}{\partial \hat{t}} = \frac{\partial}{\partial \hat{x}}\left(\frac{\hat{h}^3}{3}\frac{\partial \hat{p}}{\partial \hat{x}} - \frac{\hat{h}^2}{2}\right). \tag{10}$$

Returning to the $\hat{y}$-momentum equation (5), integration in $\hat{y}$ and enforcing the Young-

Laplace equation on the free surface yields

$$\hat{p}\left(\hat{x},\hat{y},\hat{t}\right)=\hat{p}_0+\hat{g}\left(\hat{h}\left(\hat{x},\hat{t}\right)-\hat{y}\right)-\hat{\gamma}\frac{\partial^2\hat{h}}{\partial\hat{x}^2} \tag{11}$$

and thus

$$\frac{\partial\hat{p}}{\partial\hat{x}}=\hat{g}\frac{\partial\hat{h}}{\partial\hat{x}}-\hat{\gamma}\frac{\partial^3\hat{h}}{\partial\hat{x}^3}; \tag{12}$$

here we assume that $\left(\frac{\partial\hat{h}}{\partial\hat{x}}\right)^2\ll 1$, and hence the total curvature is about $-\frac{\partial^2\hat{h}}{\partial\hat{x}^2}$. Using this in equation (10), we arrive at the thin film equation in the presence of a wind shear,

$$\frac{\partial\hat{h}}{\partial\hat{t}}=\frac{\partial}{\partial\hat{x}}\left(\frac{\hat{h}^3}{3}\left(\hat{g}\frac{\partial\hat{h}}{\partial\hat{x}}-\hat{\gamma}\frac{\partial^3\hat{h}}{\partial\hat{x}^3}\right)-\frac{\hat{h}^2}{2}\right). \tag{13}$$

In the application of oil film interferometry in a wind tunnel, order of magnitude estimates show that gravitational and surface tension effects are negligible. Assuming a silicone oil film with a thickness scale of 2 μm (about 5 optical wavelengths in oil) and a streamwise length scale of 2 cm, Blasius shear stress calculations show that up to a flat plate length of 10 m, the wind tunnel speed must be 0.02 $\frac{\mathrm{m}}{\mathrm{s}}$ or lower for the gravitational and shear stress terms to be non-negligible. Since this is virtually never the case, the wind shear thin film equation reduces to

$$\frac{\partial\hat{h}}{\partial\hat{t}}=-\hat{h}\frac{\partial\hat{h}}{\partial\hat{x}}, \tag{14}$$

This partial differential equation has a separable solution

$$\hat{h}\left(\hat{x},\hat{t}\right)=\frac{\hat{x}+k_1}{\hat{t}+k_2}, \tag{15}$$

where the k_i terms are constants appropriately chosen to meet boundary conditions. Choosing $\hat{x}=0$ to the point at which the film starts, we obtain

$$\hat{h}\left(\hat{x},\hat{t}\right)=\frac{\hat{x}}{\hat{t}+\left(\frac{\partial\hat{h}}{\partial\hat{x}}\right)_0^{-1}} \tag{16}$$

$$-\frac{1}{\hat{h}}\frac{\partial\hat{h}}{\partial\hat{t}}=\frac{\partial\hat{h}}{\partial\hat{x}}=\frac{1}{\hat{t}+\left(\frac{\partial\hat{h}}{\partial\hat{x}}\right)_0^{-1}} \tag{17}$$

where $\left(\frac{\partial \hat{h}}{\partial \hat{x}}\right)_0$ is the value of $\frac{\partial \hat{h}}{\partial \hat{x}}$ at zero time and any horizontal location.

We return now to dimensional quantities. When employing oil film interferometry, the fringe spacing s is the streamwise distance between consecutive regions of constructive interference, where the light reflected off the oil surface and the light reflected off the wall are in phase. For the two beams to be in phase, we require that h be an integral multiple of $\frac{\lambda}{2n}$, half the optical wavelength in the oil. Since equation (16) shows h to be linear in x, consecutive fringes are horizontally spaced apart by $s\left(t\right)$ and vertically by a constant

$$h\left(x_0 + s\left(t\right), t\right) - h\left(x_0, t\right) = \frac{\lambda}{2n}. \tag{18}$$

The linearity of h in x implies

$$\frac{\partial h}{\partial x} = \frac{\lambda}{2sn}; \tag{19}$$

substitution in equation (14) yields

$$\tau = -\frac{2n\mu s}{\lambda h}\frac{\partial h}{\partial t}. \tag{20}$$

Using the dimensional form $h\left(x,t\right) = x\left(\frac{\tau t}{\mu} + \left(\frac{\partial h}{\partial x}\right)_0^{-1}\right)^{-1}$ in equation (18), we find

$$\frac{s\left(t\right)}{\frac{\tau t}{\mu} + \left(\frac{\partial h}{\partial x}\right)_0^{-1}} = \frac{\lambda}{2n} \tag{21}$$

$$s\left(t\right)\frac{h\left(x,t\right)}{x} = \frac{\lambda}{2n} \tag{22}$$

$$\frac{\partial s}{\partial t}h + s\frac{\partial h}{\partial t} = 0, \qquad \text{(differentiation in } t\text{)} \tag{23}$$

and substitution for $-\frac{s}{h}\frac{\partial h}{\partial t}$ in (20) finally yields the oil film interferometry equation,

$$\tau = \frac{2n\mu}{\lambda}\frac{ds}{dt}. \tag{24}$$

3 Effect of 1-D surface roughness

3.1 Derivation

Suppose now that the we wish to use oil film interferometry in a wind tunnel, but the test surface is rough. For simplicity, we assume a 1-D surface roughness $y = f\left(x\right)$ with low magnitude compared

to h; we aim to derive an equation for $h(x,t)$ and comment on the use of oil film interferometry in this case. Once again, we nondimensionalize lengths by a constant inverse length k. Ideally, k should be associated with the length of some feature in $f(x)$, as in the examples in Section 3.2 and 3.3.

It turns out that the expression for $\hat{h}$ can be derived without considering the vertical velocity $\hat{v}$; however, we leave equations for $\hat{v}$ here so that the internal flow field can ultimately be solved. As in the case of the smooth wall, the flow under consideration is non-inertial to very good approximation, because of the very small velocity and length scales involved. Thus,

$$0 = \frac{\partial \hat{u}}{\partial \hat{x}} + \frac{\partial \hat{v}}{\partial \hat{y}} \tag{25}$$

$$0 = -\frac{\partial \hat{p}}{\partial \hat{x}} + \frac{\partial^2 \hat{u}}{\partial \hat{y}^2} \tag{26}$$

$$0 = -\frac{\partial \hat{p}}{\partial \hat{y}} + \frac{\partial^2 \hat{v}}{\partial \hat{y}^2} - \hat{g}. \tag{27}$$

These equations are subject to the boundary conditions

$$0 = \hat{u}\left(\hat{x}, \hat{f}(\hat{x}), \hat{t}\right) \tag{28}$$

$$0 = \hat{v}\left(\hat{x}, \hat{f}(\hat{x}), \hat{t}\right) \tag{29}$$

$$1 = \frac{\partial \hat{u}}{\partial \hat{y}}\left(\hat{x}, \hat{h}(\hat{x},\hat{t}), \hat{t}\right) + \frac{\partial \hat{v}}{\partial \hat{x}}\left(\hat{x}, \hat{h}(\hat{x},\hat{t}), \hat{t}\right). \tag{30}$$

If $\hat{x}$ scales by some horizontal length $\hat{l}$ and $\hat{y}$ by $\hat{h}$, then continuity (equation (25)) implies a scaling $\hat{v} \sim \frac{\hat{u}\hat{h}}{\hat{l}}$. This is generally true provided that $\hat{h} \gg \hat{f}$ and horizontal features of $\hat{f}$ are much larger than vertical features. From this, we also find that $\frac{\partial \hat{u}}{\partial \hat{y}} \sim \frac{\hat{u}}{\hat{h}} \gg \frac{\hat{u}\hat{h}}{\hat{l}^2} \sim \frac{\partial \hat{v}}{\partial \hat{x}}$. Hence, the free surface boundary condition reduces to

$$1 = \frac{\partial \hat{u}}{\partial \hat{y}}\left(\hat{x}, \hat{h}(\hat{x},\hat{t}), \hat{t}\right). \tag{31}$$

To attach a figure to the horizontal velocity scale, we appeal to the result in equation (9) that in the absence of a pressure gradient, $\hat{u} \sim \frac{\hat{h}}{2}$. (In the presence of surface roughness, we do not expect this scale to change drastically.) From this, we find that the diffusive term in the y-momentum equation (27) is insignificant if $\frac{\hat{v}}{\hat{h}^2} \ll \hat{g}$, or equivalently, $2\hat{l}\hat{g} \gg 1$. Given a typical

$l = 2$ cm and $\rho = 1000\ \frac{\text{kg}}{\text{m}^3}$, this corresponds to $\tau \ll 400$ Pa, which is virtually always the case in oil film experiments. Thus we reduce the y-momentum equation to $0 = -\frac{\partial \hat{p}}{\partial \hat{y}} - \hat{g}$, which yields

$$\hat{p}\left(\hat{x}, \hat{y}, \hat{t}\right) = \hat{p}_0 + \hat{g}\left(\hat{h}\left(\hat{x}, \hat{t}\right) - \hat{y}\right) - \hat{\gamma}\frac{\partial^2 \hat{h}}{\partial \hat{x}^2}, \tag{32}$$

exactly as in equation (11).

Hence, $\frac{\partial^2 \hat{p}}{\partial \hat{x} \partial \hat{y}} = 0$, and we conclude that $\frac{\partial \hat{p}}{\partial \hat{x}}$ is independent of $\hat{y}$. Integration of the $\hat{x}$-momentum equation (26) twice in $\hat{y}$ and using the above equation for pressure yields

$$\hat{u}\left(\hat{x}, \hat{y}, \hat{t}\right) = \left(\hat{g}\frac{\partial \hat{h}}{\partial \hat{x}} - \hat{\gamma}\frac{\partial^3 \hat{h}}{\partial \hat{x}^3}\right)\frac{\hat{y}^2}{2} + c_1\left(\hat{x}, \hat{t}\right)\hat{y} + c_2\left(\hat{x}, \hat{t}\right). \tag{33}$$

Turning again to the previous scaling (i.e., $h = 2$ μm and $l = 2$ cm), and this time adding additional typical scales $\gamma = 0.02\ \frac{\text{N}}{\text{m}}$, and $\mu = 0.02\ \frac{\text{kg}}{\text{ms}}$, we find that $\frac{\tau}{k\mu}\left(\hat{g}\frac{\partial \hat{h}}{\partial \hat{x}} - \hat{\gamma}\frac{\partial^3 \hat{h}}{\partial \hat{x}^3}\right)\frac{\hat{y}^2}{2}$ is in the rough vicinity of $10^{-10}\ \frac{\text{m}}{\text{s}}$, far less than the expected velocity scale. Elimination of this nonlinear term and applying the no-slip condition in equation (28), we obtain $\hat{u}\left(\hat{x}, \hat{y}, \hat{t}\right) = c_1\left(\hat{x}, \hat{t}\right)\left(\hat{y} - \hat{f}\left(\hat{x}\right)\right)$. Using equation (31) to solve for c_1, we reduce this to

$$\hat{u}\left(\hat{x}, \hat{y}\right) = \hat{y} - \hat{f}\left(\hat{x}\right). \tag{34}$$

Using this result in the continuity equation (25), we find that given the no-slip condition on v (equation (29)),

$$\frac{\partial \hat{v}}{\partial \hat{y}} = \hat{f}'\left(\hat{x}\right) \tag{35}$$

$$\hat{v}\left(\hat{x}, \hat{y}\right) = \hat{f}'\left(\hat{x}\right)\left(\hat{y} - \hat{f}\left(\hat{x}\right)\right). \tag{36}$$

If we set $\dot{\hat{x}} = \hat{u}$ and $\dot{\hat{y}} = \hat{v}$, then the streamlines can be found from equations (34, 36) to be $\hat{y} = \hat{y}_0 + \hat{f}\left(\hat{x}\right) - \hat{f}\left(\hat{x}_0\right)$, with $\left(\hat{x}_0, \hat{y}_0\right)$ as the initial condition.

As an aside, it is prudent at this point to check the previous assumption that the inertial terms in the Navier-Stokes equations are in fact negligible. In the above derivation, we first state that diffusive terms are of much greater scale than inertial terms, but we later find that the diffusive

terms are zero. Using the above expressions for $\hat{u}$ and $\hat{v}$,

$$\hat{u}\frac{\partial \hat{u}}{\partial \hat{x}} + \hat{v}\frac{\partial \hat{u}}{\partial \hat{y}} = 0 \tag{37}$$

$$\hat{u}\frac{\partial \hat{v}}{\partial \hat{x}} + \hat{v}\frac{\partial \hat{v}}{\partial \hat{y}} = \hat{f}''\left(\hat{x}\right)\left(\hat{y} - \hat{f}\left(\hat{x}\right)\right)^2. \tag{38}$$

This implies that the non-inertial assumption is valid in u; it is also valid in v if $Re\,\hat{f}''\left(\hat{y} - \hat{f}\right)^2 \ll 1$, where $Re = \frac{\tau}{k\mu}\frac{1}{k}\frac{1}{\nu} = \frac{\rho\tau}{k^2\mu^2}$.

The integral mass conservation equation is

$$0 = \frac{\partial\left(\hat{h} - \hat{f}\right)}{\partial \hat{t}} + \frac{\partial}{\partial \hat{x}}\left(\left(\hat{h} - \hat{f}\right)\langle\hat{u}\rangle\right), \tag{39}$$

where the cross-sectional average velocity is

$$\langle\hat{u}\rangle\left(\hat{x}\right) = \frac{1}{\hat{h} - \hat{f}}\int_{\hat{f}}^{\hat{h}}\left(\hat{y} - \hat{f}\right)d\hat{y} \tag{40}$$

$$= \frac{\hat{h} - \hat{f}}{2}. \tag{41}$$

Substitution into the mass conservation relation yields the thin film equation for oil film interferometry on a 1-D surface roughness,

$$\frac{\partial\left(\hat{h} - \hat{f}\right)}{\partial \hat{t}} = -\left(\hat{h} - \hat{f}\right)\frac{\partial\left(\hat{h} - \hat{f}\right)}{\partial \hat{x}}. \tag{42}$$

Note that although the roughness function has no dependence on time, we leave it inside the time derivative to make the thin film equation easier to solve. Equations (16–17) now hold, using $\hat{h} - \hat{f}$ in place of $\hat{h}$; the solution is

$$\hat{h}\left(\hat{x}, \hat{t}\right) = \hat{f}\left(\hat{x}\right) + \frac{\hat{x}}{\hat{t} + \left(\frac{\partial\left(\hat{h} - \hat{f}\right)}{\partial \hat{x}}\right)_0^{-1}}. \tag{43}$$

Under the approximations that have been made, this shows that the film thickness $\hat{h} - \hat{f}$ follows the same equations as in Section 2.2 (i.e., without a surface roughness). Since the

interferometry technique creates level sets of the film thickness as fringes, this implies that the oil film interferometry equation (1) should not require major changes, provided the imperfections are small compared to the film thickness. Hence, the region of the oil film near its leading edge (i.e., $\hat{x}$ close to 0) is immediately suspect, but downstream regions should not be problematic.

To create interference fringes, an incident beam (call it beam I) from the monochromatic source must be able to penetrate the oil, reflect off the imperfect surface, and transmit back to the air (beam A). This must rejoin the part of the beam that had reflects off the oil (beam B). Because $\frac{\partial(\hat{h}-\hat{f})}{\partial\hat{x}}$ is small (since this is a thin film), it is likely that a light beam that transmits through the surface, reflects off an oblique wall angle, and re-transmits (A) will have a surface-reflected counterpart (B) that reflects off a similarly oblique angle. Thus, even with surface imperfections, beams A and B should remain parallel and coincident when they rejoin, and create a fringe pattern as in Section 2.2. Hence, we can expect the oil film interferometry equation to be relatively robust. One caveat, however, is that when $\hat{f}'(\hat{x})$ becomes nontrivial, beams A and B may actually be significantly non-coincident. The severity and consequences of this non-coincidence will not be discussed here; it can be pursued in further study.

3.2 Example: single surface bump

Suppose the surface roughness is a Gaussian function, $f(x) = \epsilon\, e^{-k^2(x-x_*)^2}$, and $k\epsilon \ll 1$. If we use k^{-1} as the natural length scale as before, then $\hat{f}(\hat{x}) = \hat{\epsilon}\, e^{-(\hat{x}-\hat{x}_*)^2}$. The velocity field is

$$\hat{u} = \hat{y} - \hat{\epsilon}\, e^{-(\hat{x}-\hat{x}_*)^2} \tag{44}$$

$$\hat{v} = -2\hat{\epsilon}\,(\hat{x}-\hat{x}_*)\left(\hat{y} - \hat{\epsilon}\, e^{-(\hat{x}-\hat{x}_*)^2}\right). \tag{45}$$

This is shown in Figure 3 for $\hat{\epsilon} = 0.1$, $\hat{t} + \left(\frac{\partial(\hat{h}-\hat{f})}{\partial\hat{x}}\right)_0^{-1} = 10$, and $\hat{x}_* = 6$. The streamlines are $\hat{y} = \hat{y}_0 + \hat{\epsilon}\left(e^{-(\hat{x}-\hat{x}_*)^2} - e^{-(\hat{x}_0-\hat{x}_*)^2}\right)$.

3.3 Example: sinusoidal roughness

Assume a simple surface roughness modeled by $f(x) = \epsilon\cos(kx)$ and $k\epsilon \ll 1$. Again using k^{-1} as the length scale for nondimensionalization, $\hat{f}(\hat{x}) = \hat{\epsilon}\cos\hat{x}$ and $\hat{\epsilon} \ll 1$. This is qualitatively similar to the previous example, except that we now have an infinite number of "bumps" in the wall. The

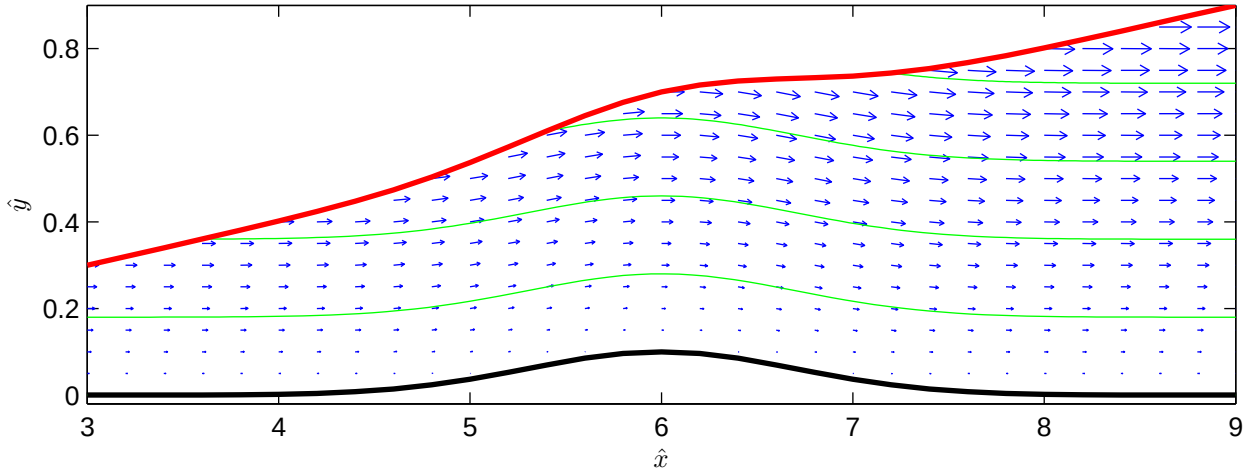

Figure 3: The velocity field in a thin film shearing over a single bump in the wall, modeled by a Gaussian curve. The wind imposes a constant shear stress τ, and $\hat{\epsilon} = 0.1$ and $\hat{t} + \left(\frac{\partial(\hat{h}-\hat{f})}{\partial \hat{x}}\right)_0^{-1} = 10$. Black: surface roughness; red: film surface; blue: velocity; green: streamlines. The vertical axis is stretched to make the vertical features of the flow more noticeable.

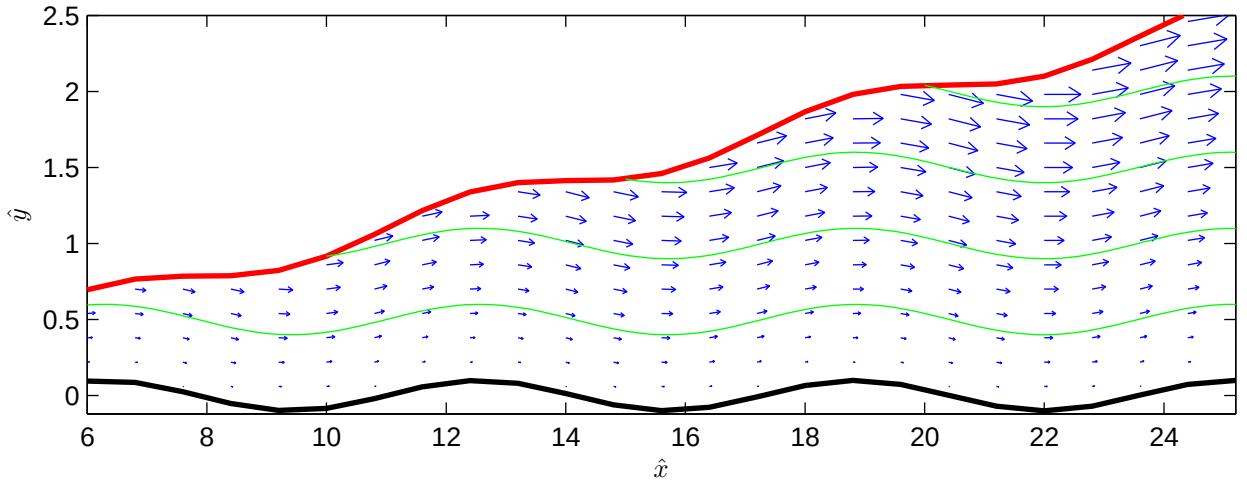

Figure 4: The velocity field in a thin film shearing over $\hat{f}(\hat{x}) = \hat{\epsilon}\cos(\hat{x})$ by a constant wind-imposed shear stress τ, with $\hat{\epsilon} = 0.1$ and $\hat{t} + \left(\frac{\partial(\hat{h}-\hat{f})}{\partial \hat{x}}\right)_0^{-1} = 10$. Black: surface roughness; red: film surface; blue: velocity; green: streamlines.

resulting nondimensional velocity field is

$$\hat{u} = \hat{y} - \hat{\epsilon}\cos\hat{x} \tag{46}$$

$$\hat{v} = -\hat{\epsilon}\sin\hat{x}\left(\hat{y} - \hat{\epsilon}\cos\hat{x}\right), \tag{47}$$

This is shown in Figure 4 for $\hat{\epsilon} = 0.1$ and $\hat{t} + \left(\frac{\partial(\hat{h}-\hat{f})}{\partial\hat{x}}\right)_0^{-1} = 10$. The streamlines are $\hat{y} = \hat{y}_0 + \hat{\epsilon}\left(\cos\hat{x} - \cos\hat{x}_0\right)$.

As previously stated, the solution for $\hat{v}$ is valid as long as $\frac{\rho\tau}{k^2\mu^2}\hat{f}''\left(\hat{y} - \hat{f}\right)^2 \ll 1$. Since both $\hat{f}$ and $\hat{f}''$ are bounded in amplitude by $\hat{\epsilon} \ll 1$, this is roughly equivalent to requiring that $\frac{\rho\tau}{k^2\mu^2}\hat{\epsilon} \ll 1$, or equivalently, $\frac{\rho\tau}{k^2\mu^2} < 10$. Using the aforementioned typical values of ρ and μ, and now also setting $k = \frac{2\pi}{1\text{ mm}}$, we find that the solution for $\hat{v}$ is valid as long as $\tau < 16$ Pa. In most applications of oil film interferometry, this shear stress limitation is satisfied.

4 Other considerations

4.1 Hysteresis

In some implementations of oil film interferometry, particularly when the wind tunnel stream speed is very low, it can take a very long time for the oil drop to develop a thin film. This raises a natural question: if we temporarily increase the tunnel speed to make the film develop more quickly, will errors be introduced into the calculated shear stress once the tunnel speed is reduced? Temporarily increasing the tunnel speed may be desirable, not only because it reduces the experimentation time, but also because the amount of airborne debris that would be implanted in the oil tends to be reduced this way. The reason for this can be explained using the scaling that the thinning rate of the oil is proportional to τ. If the stream speed U were increased by a factor of α, then in a Blasius layer, τ would be increased by $\alpha^{\frac{3}{2}}$. Thus, the time required to obtain a thin film would be modified by a factor of $\alpha^{-\frac{3}{2}}$, but the mass flux of debris would only increase by α. Thus, the total mass of debris implanted would be reduced—in principle—by $\sqrt{\alpha}$.

Using the standard set of approximations set in Section 2.2, suppose now that $U(t) = U_0 + H(t - t_*)(U_1 - U_0)$, with H the Heaviside step function. In terms of shear stress, we have $\tau(t) = \tau_0 + H(t - t_*)(\tau_1 - \tau_0)$. For the given problem, we assume that $\tau_1 < \tau_0$; τ_1 is the "desired"

shear stress, and τ_0 is a higher shear stress used to thin the film. Here, we still take $u\frac{\partial u}{\partial x} + v\frac{\partial u}{\partial y}$ to be negligible—we assume full development and the lubrication approximation. However, with a step function in a boundary condition, we no longer neglect the time derivative of u. Thus, in the absence of an externally-induced or surface tension-induced pressure gradient, the x-momentum equation (4) becomes

$$\frac{\partial u}{\partial t} = \nu \frac{\partial^2 u}{\partial y^2}, \tag{48}$$

which is the diffusion (heat) equation. The no-slip and free surface boundary conditions (equations (6, 7)) still hold, with the latter applying the expression for $\tau\,(t)$ above.

From dimensional analysis on the diffusion equation, we approximate that the timescale for diffusion to bring the thin film to a new steady state is $t \approx \frac{h^2}{\nu}$. Given a typical film thickness scale of 5 optical wavelengths in oil, or about $h = 2$ μm, this corresponds to an adjustment time scale of 200 ns. This is clearly so fast that hysteresis effects are practically nonexistent. Thus, from this analysis, we determine that it is safe (and often a good idea) to run the tunnel at a higher speed to create an oil film before acquiring data.

4.2 Error propagation from temperature

Several empirical models exist for characterizing the viscosity of an oil as a function of temperature. Common models [8] include

$$\log \mu = c_1 \log\left(T + c_2\right) + c_3 \tag{49}$$

$$\log\log \mu = c_1 T + c_2 \tag{50}$$

$$T = c_1 + c_2 \mu - \frac{c_3 \mu^2}{1 + c_4 \mu}. \tag{51}$$

To consider the error in calculated shear stress from inaccuracies in temperature measurement, we consider Dow Corning 200 silicone oils. These are readily available silicone oils that I had previously used in the experimental technique [3]. Manufacturer-provided data [9] indicates a viscosity-temperature relationship

$$\log\log\left(\beta\nu\right) = c_2 T^2 + c_1 T + c_0, \tag{52}$$

where $\beta = 2.061$ cSt^{-1}. For instance, interpolation from the specification sheet reveals a relation of $\log\log(\beta\nu) = 7.489 \cdot 10^{-6}\ \mathrm{K}^{-2}\, T^2 - 1.018 \cdot 10^{-2}\ \mathrm{K}^{-1}\, T + 3.678$ for the 20 cSt Dow Corning 200 fluid.[1]

Taking the the oil to be an incompressible fluid, a linear error propagation in the oil interferometry equation (24) yields

$$\frac{\Delta\tau}{\tau} = \frac{1}{\nu}\frac{d\nu}{dT}\,\Delta T. \tag{53}$$

Using equation (52) to determine the right-hand side derivative, we find

$$\frac{\Delta\tau}{\tau} = (2c_2T + c_1)\log(\beta\nu)\ \Delta T. \tag{54}$$

Analyzing the 10 cSt, 20 cSt, 50 cSt, 100 cSt, and 200 cSt Dow Corning 200 silicone oils[2] and determining the constants c_1, c_2, and c_3, we find that at 20 °C, these oils all follow $\frac{\Delta\tau}{\tau} = -0.022\ \mathrm{K}^{-1}\,\Delta T$ very closely. (The constant actually ranges from $-0.0223\ \mathrm{K}^{-1}$ to $-0.0213\ \mathrm{K}^{-1}$.) That is, for every degree Celsius that an experimenter's value of temperature is off, the calculated shear stress obtains a 2.2% error in the opposite direction. Although this value is determined form a linear error propagation, the function $\nu(T)$ is nearly linear in the normal operating range of 15 °C to 30 °C. This analysis shows that accurate and frequent temperature measurements are vital to the successful application of oil film interferometry. This is particularly important when wind tunnels run hot and raise the facility temperature through the course of operation.

5 Conclusion

Oil film interferometry is an inexpensive, easy, and non-intrusive method for measuring shear stress in an experimental setting, but the underlying equations require a long list of assumptions. In general, the method is robust to deviations from some of these assumptions, as demonstrated in the literature [4, 6, 7]. This study analyzes robustness in three cases—the presence of a surface roughness, hysteresis effects when the applied shear stress changes, and inaccuracy in temperature measurement.

[1] Kinematic viscosity ratings are determined at a temperature between 20 °C and 25 °C.

[2] These are sufficient for flat plate boundary layer experiments anywhere from $U \approx 3\ \frac{\mathrm{m}}{\mathrm{s}}$ to $75\ \frac{\mathrm{m}}{\mathrm{s}}$ and likely beyond, based on prior experience with the technique [3].

Ultimately, it is desirable to quantify the effects of airborne debris implantation. This phenomenon occurs commonly in many laboratories, and the extent to which debris renders the image data unusable is not well-studied. It is likely that 3-D numerical simulations would provide the most precise and systematic approach. The simulations should test debris of various sizes, from much smaller than the film height to greater than the film height. Additionally, the analysis should specifically address the effect of debris on the upstream film, where the data may still potentially be qualitatively correct (see Figure 2).

Here, we solve the simpler but related problem of a shearing oil film on an imperfect surface, where the vertical surface features are smaller in scale than the film thickness. Although this problem involves inherently different flow physics than the debris problem, it has its own applications; surfaces generally cannot be thought of as perfectly flat. By revising the thin film equation to account for the altered bottom boundary condition, it is revealed that the film thickness (which is not the same as the film height) obeys the same relations as the classical theory. In addition, the roughness should not interfere greatly with the optical measurements; only when the roughness slopes become large can the coincidence of oil-reflected and surface-reflected beams possibly become a problem.

The topic of hysteresis is one that stems from practical implementation. Often, the shear stresses to be measured are sufficiently low that the formation of an oil film may require up to half an hour or more. In this case, it is desirable first to apply a higher shear stress to create a film, and then to apply the shear stress appropriate for the experiment. A simple scaling argument shows that the oil film will settle to the new steady state within an extremely small fraction of a second of an instantaneous change in shear stress. Therefore, hysteresis effects are negligible.

Finally, a linear error analysis of Dow Corning 200 fluids, a common silicone oil, shows that for every degree Celsius that the measured temperature is off, the viscosity and hence the shear stress obtain a 2.2% error in the opposite sign. Therefore, accurate temperature sensing—as well as contamination prevention—are of utmost importance when employing this experimental technique.

Several open questions regarding non-ideal conditions still remain. For instance, Tanner [4] adjusted the thin film equation to handle situations where the pressure gradient is nonzero but small. A more complete analysis should also address any adjustments that ought to be made when the pressure gradient or $\frac{d\tau}{dx}$ is large. In addition, the thin film equation should ideally be

expanded to two dimensions, because the real-life application of oil film interferometry has two clear horizontal directions—one parallel to the shear, and one perpendicular. A two-dimensional film analysis would allow us to address additional considerations, such as the effect when an oil drop is particularly large or small. Finally, the 1-D surface roughness analysis assumed that the vertical features of the roughness are significantly smaller than the film height. This condition is always violated near the edge of the film, so film edge effects should be studied as well.

References

[1] H. H. Fernholz et al. New developments and applications of skin-friction measuring techniques. *Measurement Science and Technology*, 7(10):1396–1409, October 1996.

[2] L. C. Squire. The motion of a thin oil sheet under the steady boundary layer on a body. *Journal of Fluid Mechanics*, 11(2):161–179, September 1961.

[3] K. K. Chen. Measurements of the effects of grid wind turbulence on wall shear stress by oil film interferometry. Technical report, California Institute of Technology, September 2005. For completion of the Summer Undergraduate Research Fellowships program, under the advising of Morteza Gharib and Brad Dooley.

[4] L. H. Tanner and L. G. Blows. A study of the motion of oil films on surfaces in air flow, with application to the measurement of skin friction. *Journal of Physics E: Scientific Instruments*, 9(3):194–202, March 1976.

[5] J. D. Ruedi, H. Nagib, J. Österlund, and P. A. Monkewitz. Evaluation of three techniques for wall-shear measurements in three-dimensional flows. *Experiments in Fluids*, 35(5):389–396, November 2003.

[6] J. W. Naughton and M. Sheplak. Modern developments in shear-stress measurement. *Progress in Aerospace Sciences*, 38(6–7):515–570, August–October 2002.

[7] G. Janke. *Über die Grundlagen und einige Anwendungen der Ölfilm-interferometrie zur Messung von Wandreibungsfeldern in Luftströmungen.* PhD thesis, Technische Universität Berlin, 1993.

[8] R. G. Sloane and C. Winning. Viscosity-temperature relationship of lubricating oils. *Industrial and Engineering Chemistry*, 23(6):673–674, June 1931.

[9] Dow Corning. *Viscosity-Temperature Relationships*. Specification sheet for Dow Corning 200 silicone oils.